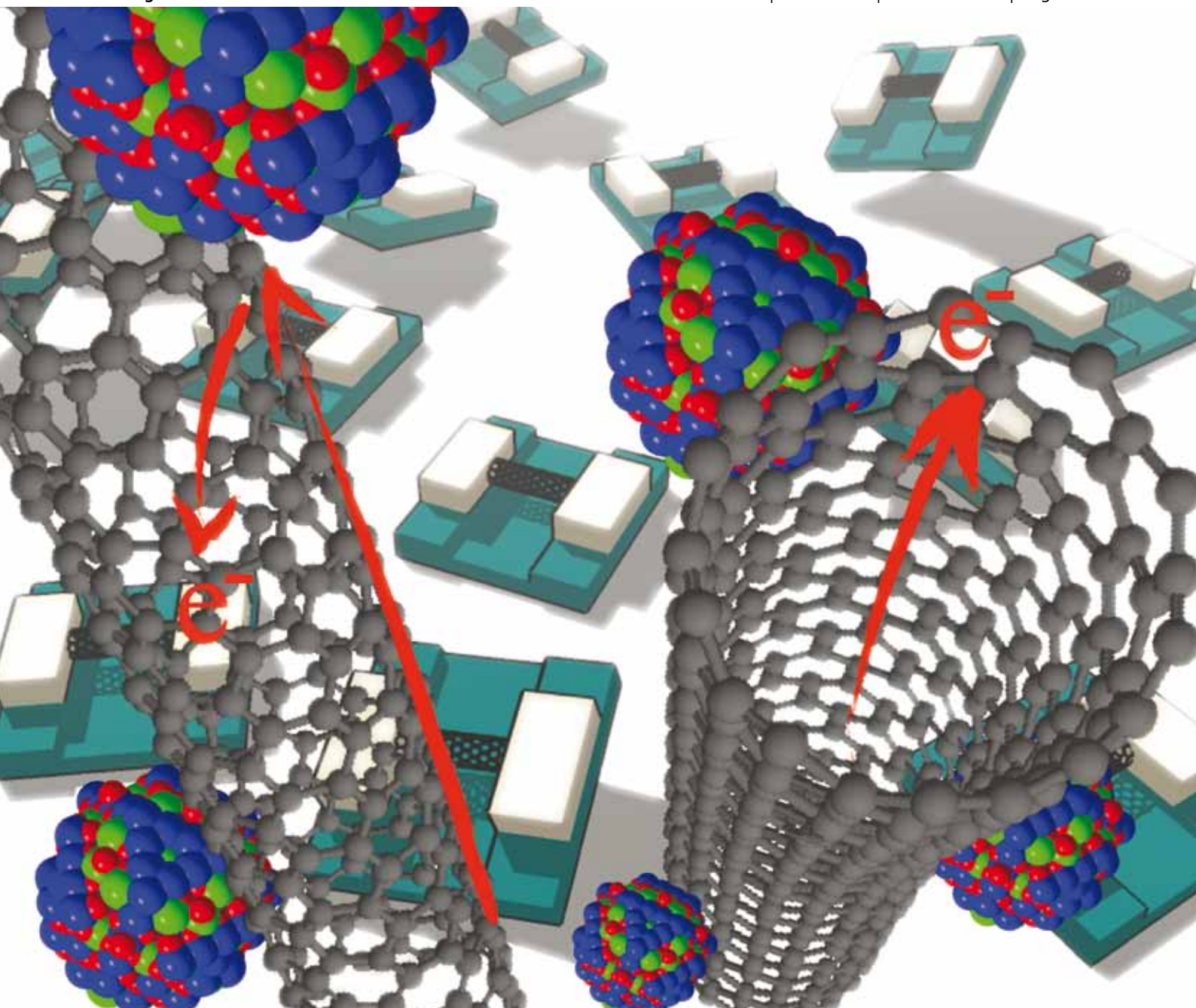


Journal of Materials Chemistry

www.rsc.org/materials

Volume 20 | Number 11 | 21 March 2010 | Pages 2041–2252



ISSN 0959-9428

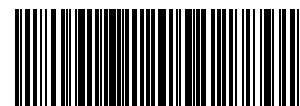
RSC Publishing

PAPER

Lapo Bogani *et al.*
Effect of sequential grafting of
magnetic nanoparticles onto metallic
and semiconducting carbon-nanotube
devices

HIGHLIGHT

Jennifer M. Pringle *et al.*
Organic ionic plastic crystals: recent
advances



0959-9428(2010)20:11;1-T

Effect of sequential grafting of magnetic nanoparticles onto metallic and semiconducting carbon-nanotube devices: towards self-assembled multi-dots†

Lapo Bogani,^{*ab} Romain Maurand,^a Laëtitia Marty,^a Claudio Sangregorio,^c Claudia Altavilla^d and Wolfgang Wernsdorfer^a

Received 18th August 2009, Accepted 4th December 2009

First published as an Advance Article on the web 4th February 2010

DOI: 10.1039/b917111h

We demonstrate that van der Waals interactions can be used to self-assemble a small, controlled number of magnetic nanoparticles onto metallic and semiconducting carbon nanotubes. We study the effect of the sequential grafting on the room temperature transport properties of carbon-nanotube electronic devices containing metallic or semiconducting carbon nanotubes. The results show that the grafting of the nano-objects has different effects on metallic and semiconducting CNTs, with an appreciable effect for single nanoparticle grafting only on field effect transistors. The results indicate that these grafting techniques are suited for the production of multi-quantum dot systems usable at low temperatures. Magnetization measurements of single nano-objects using carbon nanotube-based magnetic sensors, like nano-SQUID devices, also become feasible.

Obtaining electronic devices constituted of a few nano-objects with different functionalities is an essential issue of modern electronics¹ and in the emerging field of molecular spintronics,² where a controlled number of nanomagnets must be coupled to an electronic nanodevice. Systems with a quantized energy spectrum, called quantum dots (QDs), can be considered as artificial atoms and display quantum transport properties.³

One way to perform molecular spintronic measurements is to use break junctions, in which a single magnetic molecule or QD is sandwiched between two metallic electrodes inside a nanometre-sized gap.² Another possibility is to use the tip of a scanning tunneling microscope to let a current flow through the molecule or QD. All such measurements descend from single molecule transport experiments, and can rely on previous experience and background. Anyway in these detection schemes the electron flow interacts strongly with the probed system, even altering its oxidation state. Such changes could be exploited, in molecular magnets, to observe interesting physical effects, *e.g.* negative differential conductance,⁴ but undoubtedly alter the magnetic state of the probed system. In contrast, it is important, *e.g.* to perform quantum computation experiments, to be able to probe the magnetization of a magnetic QD without interacting too strongly with it.

Under this perspective it must be noticed that in spintronic experiments, unlike purely electrical transport spectroscopy, we do not necessarily need to flow the electrons through the

molecule. If the magnetization of the nanomagnet can affect the electron flow through a nearby object, then we can probe the magnetization of the single object without strongly altering the magnetic state. This detection scheme uses what we called a spintronic double-dot,² and a proposed implementation exploits the particular properties of carbon nanotubes (CNTs).²

CNTs constitute one-dimensional conducting nanowires and are appealing constituents for such double-dot hybrids as they behave, in small junctions, as QDs.⁵ They display semi-conducting or metallic behaviour, depending on their structural characteristics. It is thus possible to build a variety of circuits from single CNTs, and obtain CNT-based field effect transistors (CNT-FETs)⁶ or CNT-based superconducting quantum interference devices (CNT-SQUIDs),⁷ depending on the contacts used and the CNT connected. The absence of an outer oxide layer, normally present on nanowires and on most inorganic nanostructures, makes such devices particularly sensitive. CNT devices thus constitute extremely sensitive probes for chemical and biological applications^{8,9} and CNT-based SQUIDs are, in principle, sensitive enough to probe the magnetization of a single nanoparticle (NP), molecule or atom.⁷ With one magnetic QD in the multi-dot device, such CNT-based circuits could be used for molecular spintronics experiments,² provided that the QDs interact only weakly, thus retaining their identity.^{2,7}

Coupling a single, integrated CNT with a controlled number of nanomagnets, thus forming a multi-dot device, is a fundamental step towards information processing and advanced nano-electronics.¹⁰ The controlled assembly of multi-dots is still a challenging task, and the inclusion of a magnetic QD is almost unconsidered. Chemical methods have produced double- and multi-dots useful for optical investigation¹¹ and multi-QDs suitable for transport measurements have been created with lithographic techniques.¹² Anyway scaling these fabrication processes up to more than a few QDs has proved to be a formidable task, and the processes are usually not suited to magnetic materials. Thus new ways have to be explored for molecular spintronics.

^aInstitut Néel, CNRS, 25 Rue des Martyrs, 38042 Grenoble, France; Fax: +33 0476881191; Tel: +33 0476887909

^b1. Physikalisches Institut, Universität Stuttgart, Pfaffenwaldring 57, 70550 Stuttgart, Germany. E-mail: lapo.bogani@pi1.physik.uni-stuttgart.de.; Fax: +49 071168564886; Tel: +49 071168564791

^cDepartment of Chemistry and INSTM research unit, La.M.M. laboratory, Università di Firenze, Via della Lastruccia 3, 50019 Sesto Fiorentino (FI), Italy; Fax: +39 0554573372; Tel: +39 0554573338

^dDipartimento di Scienze Chimiche, Università di Catania, V.le A. Doria 6, 95125 Catania, Italy

† Electronic supplementary information (ESI) available: Control experiments on CNT-FETs. See DOI: 10.1039/b917111h

Here we show how this problem can be efficiently solved by using CNTs and developing specifically-designed nanomaterials allowing a controlled self-assembly of multi-dot hybrid devices. We characterize the electronic properties of such hybrids at room temperature on varying the number of grafted QDs, and considering metallic and semiconducting CNTs. We show that while the grafting of a single QD produces appreciable effects on devices made of semiconducting CNTs, metallic CNTs are much less affected, allowing for the use of the multi-QDs at low temperatures in ultrasensitive devices.

Experimental

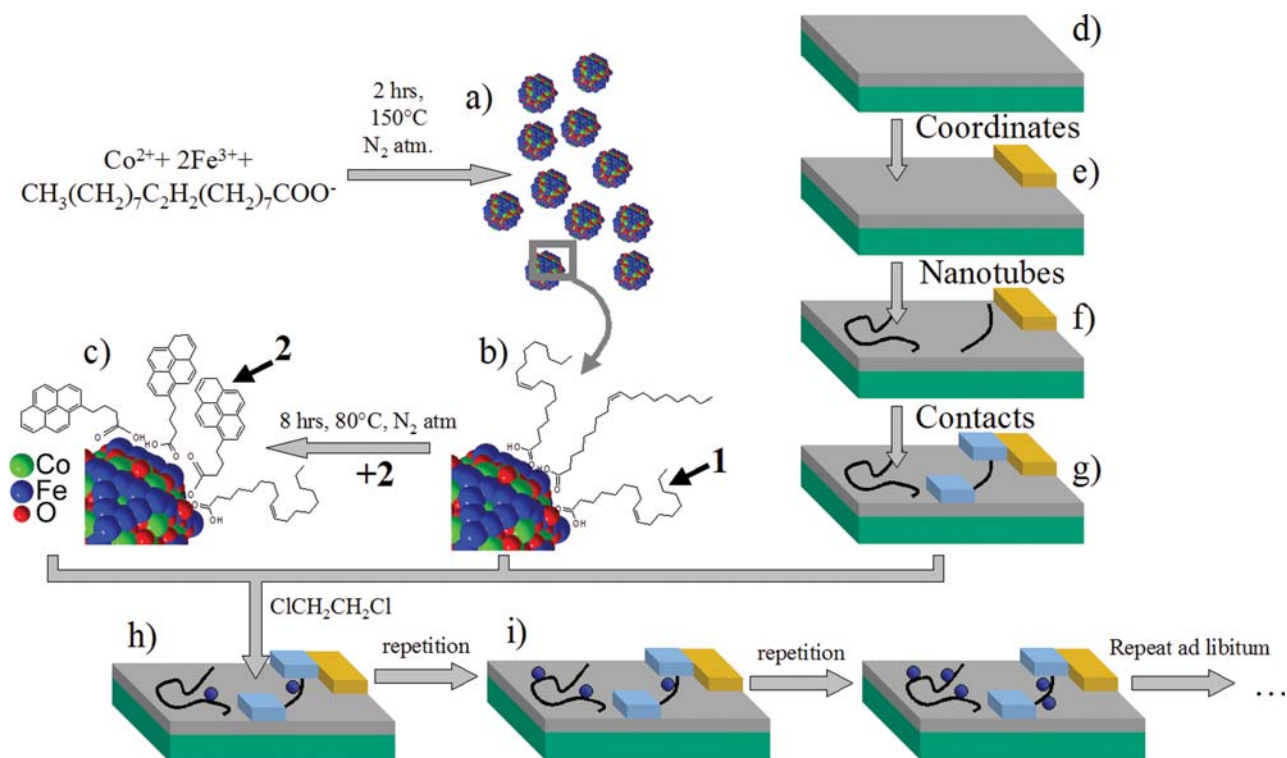
Synthesis of the NPs

The magnetic NPs are synthesized as follows: $\text{Fe}(\text{acac})_3$ (2 mmol), $\text{Co}(\text{acac})_3$ (1 mmol), 1,2-hexadecanediol (10 mmol), oleic acid (**1**) (6 mmol), oleylamine (6 mmol), and phenyl ether (20 mL) are mixed and heated to 200 °C for 30 min under a flow of N_2 . Under a blanket of N_2 the mixture is heated to reflux (265 °C) for another 30 min and then cooled down to room temperature. Under ambient conditions, ethanol (40 mL) is added to the mixture, and a black material is precipitated and separated *via* centrifugation. The sample is then washed with toluene. Part of the product is then dissolved in a dichloromethane–toluene 2 : 1 deoxygenated mixture and an excess of 4-(1-pyrenyl)butanoic acid (**2**) is added. The mixture is heated at 80 °C under N_2 atmosphere for 8 h to exchange a portion of the surface molecules of **1** with **2**. The solvent is then evaporated

under reduced pressure and the precipitate is washed with ethanol and propanol, so as to remove any excess of **1** and **2**.

Fabrication of the CNT-based electronic devices

The CNT-based electronic circuits are fabricated on degenerately n-doped Si wafers covered with a 300 nm thick SiO_2 layer (Siltronix sas), as represented in Scheme 1. Gold electrodes are fabricated on the surface by deep-UV lithography. This first pattern also provides a reference system to locate the CNTs on the surface. The surface is then coated with a monolayer of 3-aminopropyltriethoxysilane (APTES) by exposure to APTES vapour under reduced pressure (1 mbar) and in a controlled atmosphere. HiPCo single-walled CNTs are added to a solution of sodium dodecylsulfate (SDS) in water and sonicated for 15 min, obtaining a homogeneous dispersion. This CNT dispersion is then centrifuged at 3000 rpm for 30 min and additionally allowed to settle for about 15 days. The CNTs are then attached to the APTES-functionalized surface by immersing the wafer and then retracting it at a speed of $10 \mu\text{m min}^{-1}$. Inspection of the surface indicates that the procedure affords good combing, with most of the CNTs aligned along the direction of retraction. From the atomic force microscopy (AFM) heights isolated CNTs are frequently found on the surface, as well as some bundles. Individual CNTs are then located, using AFM, and their position is noted with respect to the gold reference frame. This allows them to be connect, using e-beam lithography, with Pd electrodes separated by 300 nm wide gaps.



Scheme 1 Assembly of the hybrids. CoFe_2O_4 magnetic nanoparticles are synthesized (a). Their surface is functionalized either with oleic acid, **1** (b), or 4-(1-pyrenyl)butanoic acid, **2** (c). (d) Si wafers (green) covered by a SiO_2 layer (gray) are used to fabricate gold electrodes (orange) (e). CNTs are then deposited, located with AFM (f), and individually connected with Pd leads (azure) spaced by 300 nm (g). Selective grafting of the NPs on CNTs yields the hybrids (h). Successive depositions allow control over the number of NPs in the hybrids (i).

Grafting of the NPs on CNTs

NPs are first dispersed in 1,2-dichloroethane (dce) and the nano-hybrids are then produced by submerging the circuits for about 300 s into the dispersion of the NPs and finally washing in flowing dce for 30 s. The procedure is repeated several times, imaging the single CNTs by AFM after the treatments. The same method is performed on different samples, using the same experimental conditions, for NPs covered with both **1** and **2**.

Characterization

The magnetic properties of the NPs were measured using a Cryogenics S600 SQUID magnetometer. All measurements were corrected for the diamagnetic contribution of the sample holder and the matrix, as independently determined. The topographic analysis was performed with a Veeco D3100 AFM with closed-loop feedback in tapping mode. The transmission electron microscopy (TEM) characterization was performed with a JEM 2010 electron microscope operating at 200 kV. The X-ray characterization was performed with a Bruker D8 Advance diffractometer with Cu-K α radiation.

Results and discussion

Characterization of the CoFe₂O₄ nanoparticles

We decided to decorate the CNTs with NPs of CoFe₂O₄, which is a semiconductor with a 0.8 eV bandgap¹³ and cannot undergo further oxidation, which could alter the magnetic and electronic properties. Moreover CoFe₂O₄ NPs usually possess large hysteresis cycles, thus releasing large amounts of energy during the magnetization reversal process.¹⁴ TEM inspection, reported in Fig. 1, reveals a precipitate composed of high-quality spherical NPs and evaluation of the dimensions of the NP metallic cores establishes a rather narrow size dispersion, well reproduced ($R^2 = 0.902$) by a log-normal distribution with mean diameter $\langle D \rangle = 6.1 \pm 1.7$ nm (see further on in comparison with AFM data). X-Ray measurements show the presence of well-defined Bragg peaks, indicating that the precipitate is composed of high-quality monocrystalline CoFe₂O₄ NPs with spinel structure.

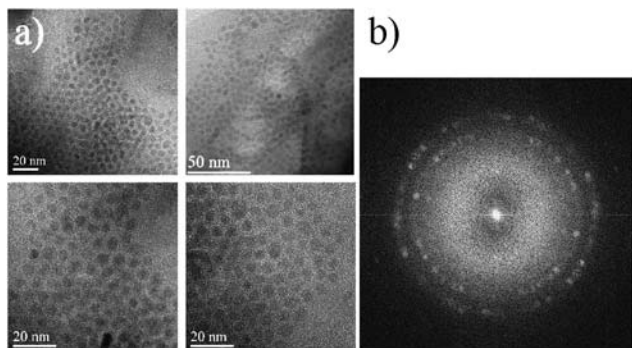


Fig. 1 Structural characterization of the NPs. (a) Transmission electron microscopy images taken at different magnifications, revealing NPs with a narrow size distribution and spherical shape. (b) Electron diffraction pattern of the NPs, showing the high crystallinity and the spinel structure of the NPs.

Magnetically CoFe₂O₄ NPs possess a large axial anisotropy, and strong intraparticle magnetic interactions, which make them superparamagnetic.¹⁴ NPs with axial anisotropy can be considered as giant spins having two preferential “up” and “down” orientations along the easy axis.¹⁵ Between these two energy minima corresponding to the two orientations there exists an energy barrier, which can prevent the NP from reversing its magnetization at sufficiently low temperatures. Due to this the reversal time becomes slower than the experimental timescale below the blocking temperature T_b . The energy barrier of a nanoparticle depends on its volume, on the magnetocrystalline anisotropy of the material and on other not-easily quantifiable parameters, like surface effects. Due to this reason it is thus customary to define, for a sample with an unavoidable size dispersion of the NPs, an effective anisotropy barrier K_{eff} . The magnetic properties and the superparamagnetic behaviour of our NPs are investigated using SQUID magnetometry. A zero-field cooled–field-cooled (ZFC-FC) measurement is performed (Fig. 2a) by cooling the sample in zero magnetic field $H = 0$, recording the magnetization on raising the temperature T in $H = 50$ Oe (ZFC curve), and then repeating the procedure after cooling the sample in $H = 50$ Oe (FC curve). The opening between the two curves at low temperatures clearly indicated the presence of superparamagnetic behaviour, and slow relaxation of the magnetization. The two curves become different starting at $T_b = 148$ K, which should be considered the temperature at

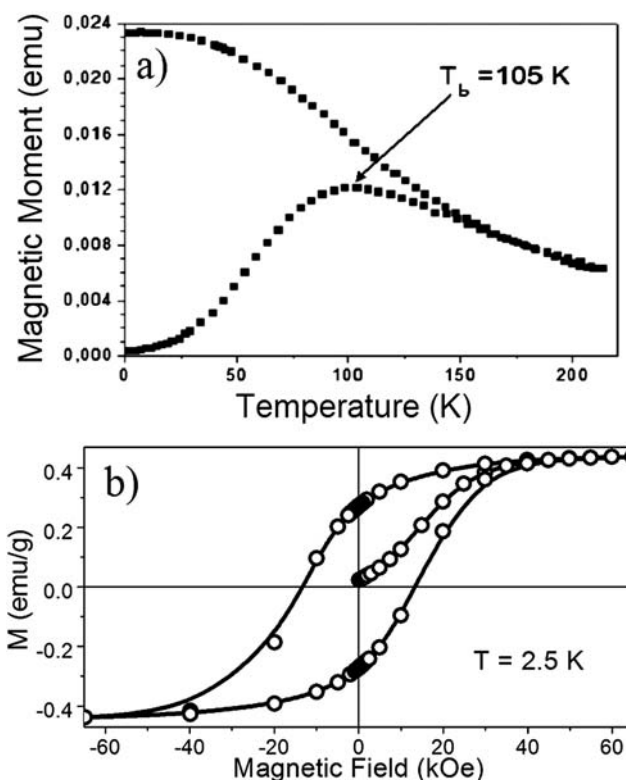


Fig. 2 Magnetic characterization of the NPs. (a) Zero-field cooled–field-cooled experiment, performed in 50 Oe, showing the blocking temperature T_b and the superparamagnetic behaviour of the NPs. (b) Magnetic hysteresis curve obtained at 2.5 K, showing the presence of a large coercive field H_c .

which the biggest NPs start showing slow relaxation of the magnetization. Anyway the average blocking temperature is usually extracted from the ZFC curve maximum, which occurs at $T_{max} = 105$ K.¹⁵ This value yields, considering the average diameter $\langle D \rangle$ using the relation $\langle K_{eff} \rangle = 150k_B T_{max} / \pi \langle D \rangle$,¹⁵ an average barrier $\langle K_{eff} \rangle = 300$ kJ m⁻³. The FC curve displays an increasing trend on lowering the temperature, which brings the magnetization value well above the maximum value of the ZFC curve. This may be due to the presence of a considerable fraction of small size NPs, as also evidenced by the TEM and AFM analysis, which leads to the complete blocking of the magnetization only below T_{max} . The low temperature curve shows a saturation value of 0.023 emu below 25 K, indicating that all NPs are blocked below this temperature. Below T_b a hysteresis cycle opens. We recorded the hysteretic behaviour of the NPs at very low temperatures ($T = 2.5$ K), where all NPs are blocked, obtaining a large coercive field $H_c = 13.1 \pm 0.1$ kOe at $T = 2.5$ K (Fig. 2b).

The structural and magnetic characterizations of the NPs thus show the characteristic features of a superparamagnetic nanostructured material, with a very large coercive field and a relatively high blocking temperature. They also allow the characterization of the structural properties of the hybrid devices, as detailed in the following section.

Structural characterization of the hybrid devices

Decoration of CNTs with QDs is an active field of research and a number of functionalization methods exist,^{16,17} mainly exploiting covalent bonds and terminal defects in the CNT. By the way covalent bonds likely produce strong coupling and, by introducing electron scattering centres, may also severely limit the performance of the devices. Terminal defects cannot evidently be used in producing electronic devices such as SQUIDS and FETs. Up to now, the non-covalent decoration of CNTs with magnetic NPs has only been performed in solution.¹⁷ These procedures graft a large number of NPs on the CNT, while no methods exist to sequentially add a small but very controlled number of nano-objects into the device, as needed for multi-dot hybrids.² Whether the ligands and methodologies used in solution remain applicable to surface-deposited CNTs and are compatible with the fabrication of electronic devices is also an open issue. Eventually, while several CNT-NP hybrid materials have been reported,^{16,17} their electronic characterizations remain largely unexplored.

Self-assembly of the hybrids after CNT connection provides two important advantages. Firstly NPs present on the CNTs before contacts are made may increase the Schottky barrier between the CNT and the leads, lowering the quality of the devices. Secondly we can progressively add NPs to the CNTs and thus characterize the hybrids after each grafting, evidencing the evolution of the properties and the applicability as a NP sensor. We thus chose to proceed with multiple treatments, grafting a few NPs each time, instead of attaching many NPs by reacting for long times.

NPs are first dispersed in dce and nano-hybrids are then produced by submerging the circuits for about 300 s into the dispersion of the NPs and finally washing in flowing dce for 150 s (Scheme 1h). The procedure is repeated several times, imaging

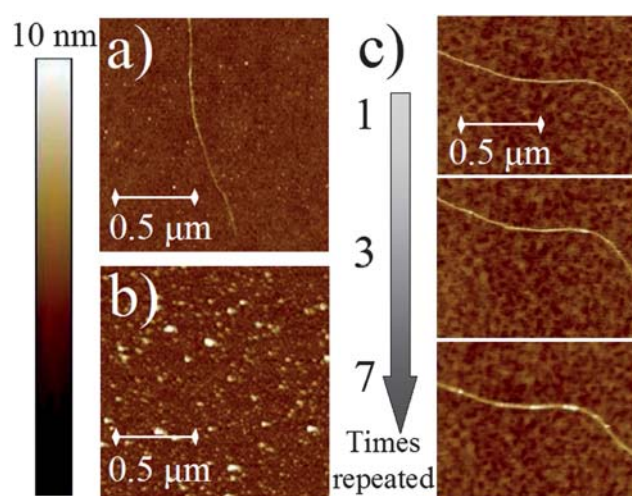


Fig. 3 AFM topography of the hybrids and demonstration of the sequential grafting. Images of the same area before (a) and after (b) treatment with NPs coated with **2**. (c) Series of images acquired on the same CNT after repeated treatment with NPs coated with **1**. The height colorbar on the left is the same for all images.

the single CNTs by AFM after the treatments (Scheme 1i). The same method is performed on different samples, using the same experimental conditions, for NPs covered with both **1** and **2**. For NPs covered with **2** the first immersion is sufficient to stick the NPs all over the surface, as reported in Fig. 3a,b. The grafting procedure is neither controlled nor selective, probably due to the fact that the surface is also covered with organic residues that cannot be efficiently cleaned without damaging the CNTs. No selectivity for the CNT is observed and reducing the NP concentration in the solution does not improve the result. In contrast, using NPs coated with **1** yields controlled and selective grafting, with only a few NPs on the CNTs, and almost none on the surface, as reported in Fig. 3c. The reason of this may lie in the different interactions afforded by the hydrophobic tail of **1**, which is a much weaker binder with respect to **2**. The fact that **1** cannot form π -stacking interactions with the CNT wall has already been exploited for medical applications,¹⁸ and may here be responsible for the better selectivity. While **2** is more efficient when grafting NPs in solution, **1** seems thus more indicated to build multi-dot materials compatibly with the fabrication of the electronic devices. Once the NPs are attached, we were not able to remove them in dce liquid, indicating that strong van der Waals forces contribute to anchoring the NPs onto the CNTs. Previous functionalization of CNT-based sensors involves first a treatment of the CNTs with pyrene-based molecules and then binding of proteins.^{8,19} Such studies lead to the immediate grafting of a relatively large number of objects,^{8,19} compared to our method. Moreover reduced reactivity is expected for small-diameter CNTs,^{18,19} which are better for electronic devices. Note that our approach allows an unprecedented sequential grafting of a controlled number of dots to the CNT, as shown by the height profile of the same CNTs on repeating the treatment with **1**-coated NPs (Fig. 4a). The statistics of the height of the grafted objects strongly resemble the NP diameter acquired with TEM (Fig. 4b). The AFM size dispersion can be fitted ($R^2 = 0.948$)

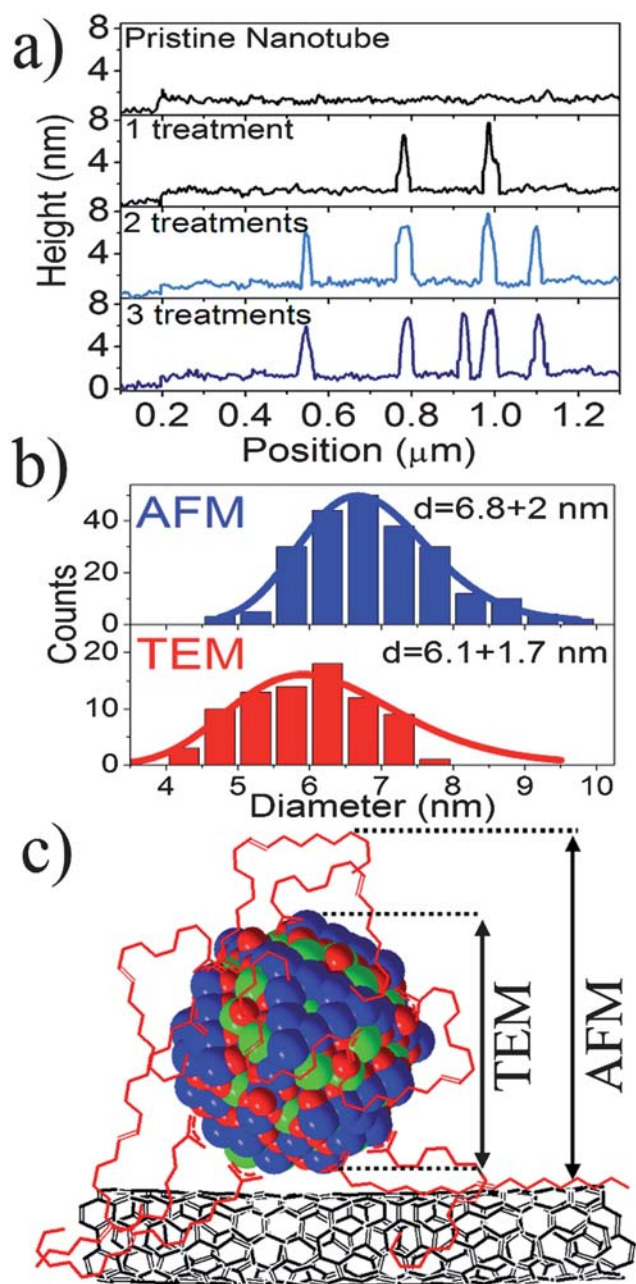


Fig. 4 Analysis of AFM topography. (a) Height profile of the same CNT, showing the sequential grafting of NPs coated with **1**. (b) Histogram of the attached NPs size, acquired as the difference between the CNT height and heights of the bumps appearing on the CNTs after treatment. The size dispersion is compared to TEM measurements. (c) Schematic representation of the origin of the difference between the NP size dispersions observed *via* TEM and AFM measurements. The NP is rendered from the observed spinel crystal structure, the oleic acid molecules are red and the CNT is black.

with a log-normal distribution peaked at 6.8 ± 2.0 nm. The fact that AFM also probes the shell of molecules surrounding the NP core (Fig. 4c) explains the small discrepancy in mean diameter. Considering the mechanical action of the AFM and the lack of a full monolayer on the NP surface, it is not surprising to find that this discrepancy is slightly smaller than the thickness of a fully-formed monolayer of **1**.

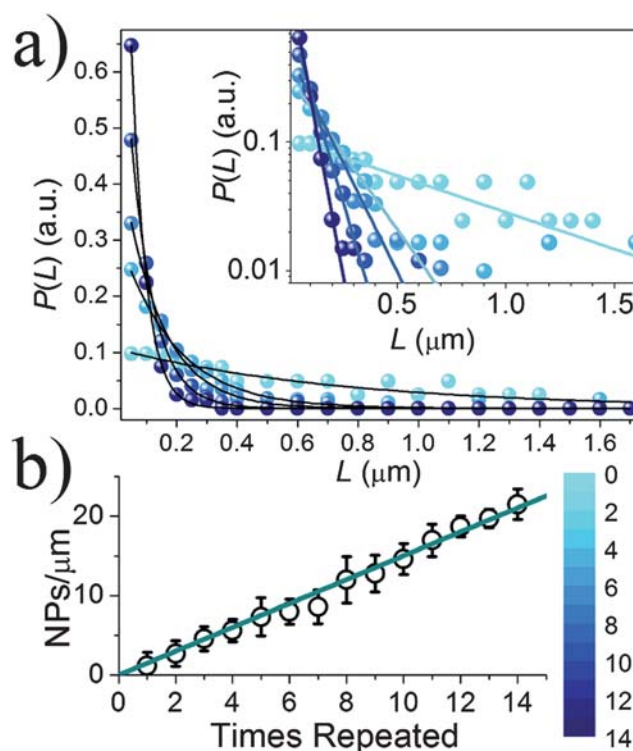


Fig. 5 Quantification of the number of NPs in the hybrids and sequentiality of the grafting. a) Probability of finding a distance L between two NPs for sequential repetitions of the process (color scale). Lines are fits to the data using the statistical distribution (see text) and different linear concentrations C of NPs per μm of CNT. The agreement with the expected distribution is highlighted in the inset. (b) Trend of C as extracted from the fits in (a), *vs.* the number of repetitions of the process. The line is a linear regression.

The fact that only a few NPs are grafted after each treatment allows control of the number of dots in the hybrids. If NPs stick randomly onto the CNT length the statistical probability P of finding a distance L between two NPs is $P(C, L) = Ce^{-LC}$, where C is the linear concentration of NPs on the CNT.²⁰ The distribution of L (Fig. 5a) is obtained by AFM observation of the same 18 CNTs (about $40 \mu\text{m}$ of total length) after each treatment. The distributions reveal good agreement with the predicted law, and the extracted C values are reported in Fig. 5b *vs.* the number of treatments, with fitting confidences as error bars. It must be noted that, by extracting C from the measurable inter-NP distances, we account for NPs that lie too close one to another to be distinguishable by the lateral resolution of the AFM. The grafting process is linear ($R = 0.997$) in the investigated range, indicating the grafting, on average, of 1.5 NP per μm for each treatment. This corresponds to the addition of about 1 NP every 2 repetitions on CNT electronic devices with 300 nm wide gaps between the leads.

This structural characterization of the hybrids thus demonstrates the selective and sequential grafting of nanomagnets into CNT-based electronic devices. Such a high level of accuracy, never attained before, is of fundamental importance for the controlled assembly of spintronic double-QDs, which must contain a controlled number of QDs in the device. As detailed in

the next section this also allows the quantification of the effect of the NP grafting on single CNT devices.

Characterization of the hybrid devices

Whatever the approach used to graft the QDs on the CNT, these will interact directly with the CNT wall, which is where the electrons flow. This is a mixed blessing as it is at the basis of the high sensitivity of CNT devices, but also means that the transport properties can be easily destroyed by the grafting.^{2,21,22}

The local variation of the potential felt by the electrons due to the grafted molecule can induce electron backscattering. This has been used, in CNT-FETs based on semiconducting CNTs, to detect single molecules grafted onto the device.^{8,9} Anyway, the same process can constitute a problem for devices that use metallic CNTs, like CNT-SQUIDS. The very symmetry of the metallic CNT band structure forbids backscattering, as long as the carrier energies are below the second subband.²³ Thus metallic CNTs show ballistic conductance, *i.e.* negligible elastic electron scattering, at room temperature over lengths as long as 1 μm , except in proximity of the Kohn anomaly. Inelastic processes, like electron-phonon scattering, can become important only for high bias voltages and high temperatures.²³ By the way, although long-range Coulomb elastic scattering is ineffective, a strong short-range potential can still lead to very efficient backscattering in metallic CNTs. Defects or molecules grafted on the CNT wall constitute typical sources of such local potentials.^{23,24} The resulting backscattering processes can produce destructive interference of the electron wavefunction, leading to a dramatic decrease of the conductivity of the CNT even for a few defective sites.^{24–26}

Such processes can be extremely detrimental for the functioning of CNT-SQUIDS. One of the main advantages of a SQUID is that it is bistable, and the magnetization reversal of the grafted object can switch one branch of the SQUID, allowing the detection of the molecular signal. If, owing to the presence of the grafted QD, the conductance in the branch is so low that the bistability is practically lost, then the device will not function.

It is thus important to develop grafting methods that, while ensuring the attachment of the nanomagnet to the CNT wall, do not introduce such strong backscattering processes in the device. By the way, while several studies deal with the effect of grafted molecules in CNT-FETs,^{8,9} few data on metallic CNTs exist.^{24–26} Experimentally, while recent irradiation studies have afforded some insight into these processes,²⁴ little is known about what functionalities can only weakly interact with the CNT electron flow, thus allowing the use of CNT-SQUIDS or analogous devices.

The electric characterization of the pristine CNT devices was performed at room temperature. The overall statistics, performed on many repetitions of the lithographic process and about 400 connected CNTs, reveal only a small percentage of actually resulted non-connected devices (<8%), or suffering from very bad contacts, with resistances above 600 k Ω . Very good contacts were in general obtained, with 65% of the devices showing resistances below 100 k Ω , most of them around 20 k Ω , which is close to the 15 k Ω resistance obtained with perfect Pd contacts on metallic CNTs. Systems with resistances lower than 100 k Ω mainly displayed metallic behaviour, with negligible field

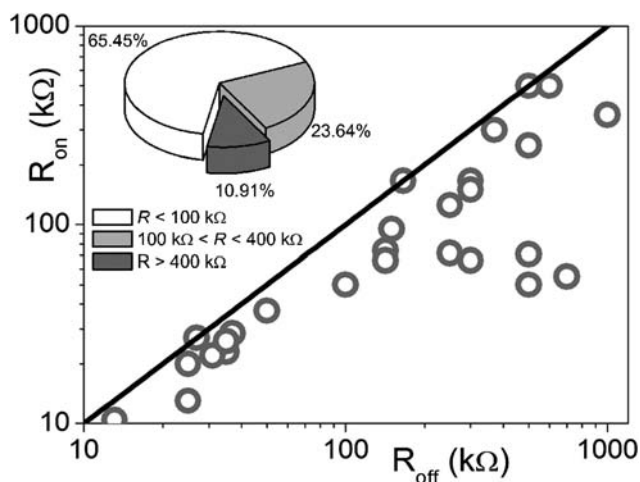


Fig. 6 Characterization of the obtained electronic devices. Bilogarithmic plot of the resistance of the ON state as a function of the resistance of the OFF state for a set of FET devices, as measured at room temperature with a 100 mV source–drain voltage. The inset shows the pie-chart of the resistances of the single-walled single-CNT FET devices. Measurements were performed at $V_g = 0$ V and with a source–drain voltage of 100 mV.

effect, while systems with resistance above 300 k Ω usually displayed field effect and hysteretic behaviour. A typical set of results is reported in Fig. 6, where we report the bilogarithmic plot of the resistances measured with a gate voltage $V_g = 30$ V (R_{on}) vs. the resistance measured at $V_g = -30$ V (R_{off}). The results reveal that a good number of the devices show a weak field effect (typically 2–3 decades), while some show perfectly metallic behaviour. Some devices showed mixed behaviour, indicating the presence of two or more CNTs connected in parallel. This may arise from the presence of small bundles, in some devices, as they cannot always be distinguished from isolated CNTs by AFM. Such devices, having ambiguous behaviour, were then excluded from further characterization.

Thanks to the controlled assembly process obtained above the electric transport properties of the hybrids were measured as a function of grafted NPs (Fig. 7a). First of all we focus on the room temperature transport properties of hybrids based on semiconducting systems, due to their interest as ultra-sensitive devices.^{8,9,19} Measurements of the current I_d vs. the gate voltage V_g show that the devices behave as p-type (ON state at $V_g < 0$) CNT-FETs with $I_{\text{ON}}/I_{\text{OFF}}$ ratios of 2–3 decades. The curves were acquired with different source–drain voltages, in the 1 μV –100 mV range, for different devices, depending on the resistance of the device under examination. The hysteretic response, characteristic of CNT-FETs on untreated SiO₂ surfaces, is due to charges injected from the CNT into the nearby region by the high electric field existing at the CNT surface for large V_g .²⁷ The subthreshold swing $S = [dV_g/d\text{Log}(I)]$, about 8 V per decade, does not change when increasing the number of NPs, indicating that the grafting does not alter the coupling to the gate. Moreover control experiments reveal no appreciable change of the response either after washing with dce alone or by treatment with 1 and then washing with flowing dce for 150 s (ESI†).

Grafted NPs act as scattering centres that hinder the electron flow through the CNT, leading to a decrease of the $I_{\text{ON}}/I_{\text{OFF}}$

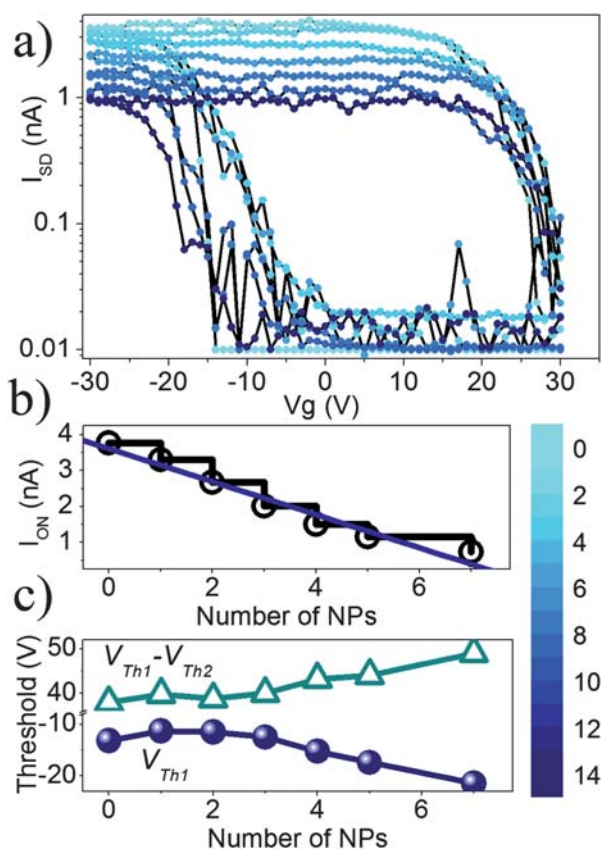


Fig. 7 Effect of NP grafting on the transport characteristics of semi-conducting CNTs. (a) Typical transfer characteristics of a CNT-FET acquired for several repetitions of the treatment (color scale). (b) Trend of I_{ON} vs. the number of NPs and linear fit to the data. The black line highlights the discrete behaviour due to the sequential grafting of NPs. (c) Width of the hysteresis (triangles) and threshold voltage V_{Th1} of the ON–OFF transition (spheres) vs. the number of NPs.

ratio. In the investigated range the I_{ON} current varies on grafting the NPs, with a quantized decrease of 0.15 nA per NP ($R = 0.989$), *i.e.* above our instrumental sensitivity of 10 pA (Fig. 7b). This demonstrates that CNT-FETs can be used as nanometric ultra-sensitive sensors with single-NP sensitivity. Previous experiments on covalently-bound proteins analogously showed single-protein sensitivity,^{8,9} yielding a I_{ON} decrease of 1 nA per protein. The I_{ON} decrease is here one order of magnitude lower, consistent with the non-covalent binding.²⁸ The NP–CNT interaction, while appreciable, is thus much less important than covalent binding and the CNT and the NPs shall be considered as interacting but still separate QDs. To give an order of magnitude the Landauer formulation in the incoherent transport regime gives an electron reflection coefficient of about 12% per NP, much lower than the 40% value reported for covalently functionalized CNTs.⁹ This value is anyway comparable with what is observed for non-covalent grafting of single-molecule magnets using pyrene functionalities, *i.e.* 7% per molecule. The fact that the grafting has a larger effect here is likely due to the presence of many oleic acid molecules on the NP surface, several of which can contribute to the grafting. The local perturbation of the energy responsible for the scattering process may then be higher and more diffuse, thus scattering the electrons more effectively.

The grafting also produces a gradual decrease in the ON–OFF threshold voltage, V_{Th1} , and an increase of the hysteresis width (Fig. 7c). Charge-trapping by the NPs and charge transfer between the NPs and the CNT can contribute to this shift. This is not surprising, as bulk CoFe_2O_4 is affected by internal charge transfers,²⁹ and atoms on the NP surface do not possess a stable environment, likely promoting electron transfer. The shift corresponds to a decrease in the effective carrier density, of 3500 holes per μm , using a backgate capacitance of $36 \text{ aF } \mu\text{m}^{-1}$ from the geometry of the device.

The effect of NP grafting on the metallic CNTs is completely different. In fact, despite the presence of high electron flows in the CNT, only a very slight decrease of the current is observed in the investigated range of grafted NPs. Anyway it must be noted that 6 QDs is a sizeable number for a multi-QD device and that the NPs are grafted into the 300 nm gap of the CNT device (Fig. 8), thus meaning an average distance of 50 nm between them. This means that the local potential produced by the NP grafting around the Fermi energy is sufficiently small that it does not produce relevant backscattering. In contrast to what happens for irradiation-induced defects, which produce defects directly in the CNT wall,²⁴ here the low intensity of the reflected waves is not capable of creating strong destructive interference, and the conductivity remains largely unaltered. Despite the different nature of the binding, this result agrees with predictions of covalently-grafted defects, for which the mean free path remains of the order of hundreds of nm for a number of grafted molecules comparable to the one used. These findings thus confirm that grafting can alter only slightly the conductivity of metallic CNT, while affecting substantially semiconducting CNTs.

While the curves going from negative to positive and from positive to negative gate voltages are completely superimposable for the pristine metallic CNT, a small hysteresis appears on grafting the NPs, indicating that the CoFe_2O_4 NPs can act as charge-traps also for metallic CNTs. By the way the effect is less discernible here, and thus not quantifiable, as in the case of semiconducting CNTs.

This feeble effect of the grafting on the metallic CNT conductivity indicates that a single grafted QD can interact with a metallic CNT in a double-dot scheme. The developed grafting

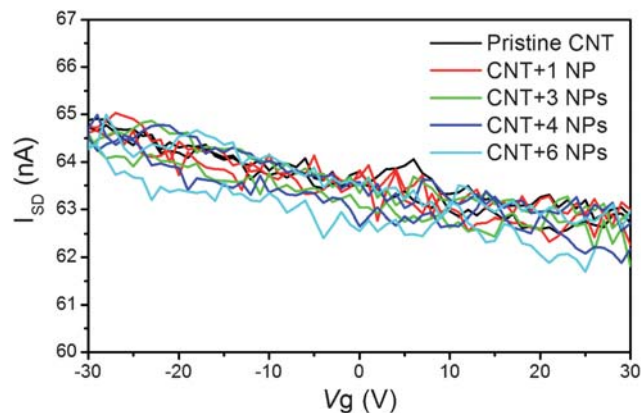


Fig. 8 Effect of NP grafting on the transport characteristics of a typical metallic CNT at room temperature. Data are acquired on the same device for several repetitions of the treatment, as indicated in the color scale, using a source–drain voltage of 1 mV.

methodology will not disrupt the electron passage through the devices at low temperature, thus allowing the functioning of devices that require good conductance, such as the nano-SQUID. While the conduction is maintained the magnetic QD can still interact perturbatively with the electron flow, for example *via* magnetic flux coupling, to produce a magnetic signal.

Conclusions

In conclusion, we described a method to controllably assemble multi-QD hybrid materials formed by CNT and magnetic NPs into working electronic devices. By combining top-down and bottom-up approaches, we have achieved the controlled self-assembly of CNT-NP multi-QDs and investigated their room-temperature transport properties. The bottom-up self-assembly techniques afford electronic devices with a controllable number of magnetic QDs, as required for the creation of molecular spintronic devices.² The conditions used are compatible with the fabrication, with top-down methods, of single-CNT electronic devices, and significant differences are found with present methods for CNT decoration in solution.

The progressive addition of QDs allowed the exploration of the evolution of the electron transport on sequentially adding NPs to the hybrids and comparison between electronic devices built of single metallic and semiconducting CNTs. The grafting has fundamentally different effects on metallic and semiconducting CNTs. Semiconducting systems, being more sensitive, allow for room-temperature single QD detection, while the grafting technique maintains the properties of metallic CNTs, which can then be used for the production of CNT-SQUID devices.

The results here reported constitute an important step towards the self-assembly of multi-QD electronic and spintronic devices. They present key advantages for the future fabrication of controlled hybrids, and allow the detection of single NPs anchored onto the CNT. The random distribution of distances between NPs, when using the CNT as a detector, should not hinder the applicability of the hybrids, in this few-QD limit. The soft-chemistry approach developed also has the advantages of being relatively inexpensive, easy to scale up for large-scale production of multi-dots and exportable to different kinds of QDs. The weak coupling between the CNT and the NPs allows the retention of the individuality of the QDs.

The results have possible applications in other areas where CNTs and NPs are increasingly employed, such as electronics, nanomedicine and biology.³⁰ Anyway the use of magnetic NPs introduces the possibility to investigate nanomagnets without strongly perturbing the magnetization dynamics, in a double-QD scheme.² Nano-SQUID characterization⁷ and magneto-Coulomb^{2,31} experiments should become feasible with the present grafting techniques. The CoFe₂O₄ NPs here used are particularly indicated, as they possess a wide magnetic hysteresis loop, corresponding to a large energy release during the magnetization reversal. As the magnetism of CoFe₂O₄ is sensitive to light irradiation²⁹ multi-QD photoswitchable devices can be envisaged. The physics of such photocommutable systems when in the Coulomb blockade regime is a promising area to explore and the self-assembly techniques developed can be further adapted for graphene-NP hybrids.³² It will also be interesting to combine

these properties with optical features, and in particular non-linear ones, as already attempted for molecular magnetic materials.³³ These developments will eventually stimulate the study of environmental effects on the magnetization dynamics.³⁴

Acknowledgements

We acknowledge Mr Uiana for the TEM characterization. The work was partially financed by the German DFG, ANR-PNANO, ANR-06-NANO-27 MolSpintronics Contract, by EC-RTN QUEMOLNA Contract MRTN-CT-2003-504880 and by MIUR (PRIN and FIRB grants). L.B. acknowledges EC Marie Curie Fellowship support *via* the EIF-041565 “MoST” grant.

Notes and references

- 1 D. M. Guldi, G. M. A. Rahman, F. Zerbetto and M. Prato, *Acc. Chem. Res.*, 2005, **38**, 871–878.
- 2 L. Bogani and W. Wernsdorfer, *Nat. Mater.*, 2008, **7**, 179–186; L. Bogani and W. Wernsdorfer, *Inorg. Chim. Acta*, 2008, **361**, 3807–3819; themed issue of *J. Mater. Chem.*, 2009, **19**, 1661–1768.
- 3 S. Tarucha, D. G. Austing, T. Honda, R. J. van der Hage and L. P. Kouwenhoven, *Phys. Rev. Lett.*, 1996, **77**, 3613–3616.
- 4 H. B. Heersche, Z. de Groot, J. A. Folk, H. S. van der Zant, C. Romeike, M. R. Wegewijs, L. Zoppi, D. Barreca, E. Tondello and A. Cornia, *Phys. Rev. Lett.*, 2006, **96**, 206801.
- 5 M. Ouyang, J.-L. Huang, C. L. Cheung and C. M. Lieber, *Science*, 2001, **292**, 702; P. Avouris, Z. Chen and V. Perebeinos, *Nat. Nanotechnol.*, 2007, **2**, 605–615.
- 6 S. J. Tans, A. R. M. Verscheuren and C. Dekker, *Nature*, 1998, **393**, 49–52; D. N. Futaba, K. Hata, T. Yamada, T. Hiraoka, Y. Hayamizu, Y. Kakudate, O. Tanaike, H. Hatori, M. Yumura and S. Iijima, *Nat. Mater.*, 2006, **5**, 987–994.
- 7 J.-P. Cleuziou, W. Wernsdorfer, V. Bouchiat, T. Ondarçuhu and M. Monthieux, *Nat. Nanotechnol.*, 2006, **1**, 53–59; P. Jarillo-Herrero, J. A. van Dam and L. P. Kouwenhoven, *Nature*, 2006, **439**, 953–956.
- 8 J. Kong, N. R. Franklin, C. Zhou, M. G. Chapline, S. Peng, K. Cho and H. Dai, *Science*, 2000, **287**, 622–625; P. G. Collins, K. Bradley, M. Ishigami and A. Zettl, *Science*, 2000, **287**, 1801–1804; K. Besteman, J.-O. Lee, F. G. M. Wiertz, H. A. Heering and C. Dekker, *Nano Lett.*, 2003, **3**, 727–730; A. Star, J. C. P. Gabriel, K. Bradley and G. Gruner, *Nano Lett.*, 2003, **3**, 459–462; R. J. Chen, S. Bangsaruntip, K. A. Drouvalakis, N. Wong Shi Kam, M. Shim, Y. Li, W. Kim, P. J. Utz and H. Dai, *Proc. Natl. Acad. Sci. U. S. A.*, 2003, **100**, 4984–4989.
- 9 Y. B. Zhang, M. Kanungo, A. J. Ho, P. Freimuth, D. van der Lelie, M. Chen, S. M. Khamis, S. S. Datta, A. T. C. Johnson, J. A. Misewich and S. S. Wong, *Nano Lett.*, 2007, **7**, 3086–3091.
- 10 W. G. van der Wiel, S. De Franceschi, J. M. Elzerman, T. Fujisawa, S. Tarucha and L. P. Kouwenhoven, *Rev. Mod. Phys.*, 2002, **75**, 1–22.
- 11 M. Ouyang and D. D. Awschalom, *Science*, 2003, **301**, 1074–1076.
- 12 J. R. Petta, A. C. Johnson, J. M. Taylor, E. A. Laird, A. Yacoby, M. D. Lukin, C. M. Marcus, M. P. Hanson and A. C. Gossard, *Science*, 2005, **309**, 2180–2184.
- 13 A. V. Ramos, T. Santos, G. X. Miao, M. J. Guittet, J.-B. Moussy and J. S. Moodera, *Phys. Rev. B: Condens. Matter Mater. Phys.*, 2008, **78**, 180402.
- 14 C. Altavilla, E. Ciliberto, A. Aiello, C. Sangregorio and D. Gatteschi, *Chem. Mater.*, 2007, **19**, 5980–5985; C. Altavilla, E. Ciliberto, C. Sangregorio and D. Gatteschi, *Adv. Mater.*, 2005, **17**, 1084.
- 15 E. C. Stoner and E. P. Wohlfarth, *Philos. Trans. R. Soc. London, Ser. A*, 1948, **240**, 599–642; M. Jamet, W. Wernsdorfer, C. Thirion, D. Mailly, V. Dupuis, P. Mélinon and A. Pérez, *Phys. Rev. Lett.*, 2001, **86**, 4676–4679.
- 16 J. M. Haremza, M. A. Hahn, T. D. Krauss, S. Chen and J. Calcines, *Nano Lett.*, 2002, **2**, 1253–1258; B. H. Juárez, C. Klinke, A. Kornowski and H. Weller, *Nano Lett.*, 2007, **7**, 3564–3568; S. Ravindran, S. Chaudhary, B. Colburn, M. Ozkan and C. S. Ozkan, *Nano Lett.*, 2003, **3**, 447–453; S. Banerjee and S. S. Wong, *J. Am. Chem. Soc.*, 2003, **125**, 10342–10350.

- 17 V. Georgakilas, D. Gournis, V. Tzitzios, L. Pasquato, D. Guldi and M. Prato, *J. Mater. Chem.*, 2007, **17**, 2679–2694; K. Kurppa, H. Jiang, G. R. Szilvay, A. G. Nasibulin, E. I. Kauppinen and M. B. Linder, *Angew. Chem., Int. Ed.*, 2007, **46**, 6446–6449; K. Jiang, A. Eitan, L. S. Schadler, P. M. Ajayan, R. W. Siegel, N. Grobert, M. Mayne, M. Reyes-Reyes, H. Terrones and M. Terrones, *Nano Lett.*, 2003, **3**, 275–277.
- 18 Z. Liu, X. Sun, N. N. Ratchford and H. Dai, *ACS Nano*, 2007, **1**, 50–56.
- 19 R. J. Chen, Y. Zhang, D. Wang and H. Dai, *J. Am. Chem. Soc.*, 2001, **123**, 3838–3839.
- 20 See, for an analogous concept: L. Bogani, A. Caneschi, M. Fedi, D. Gatteschi, M. Massi, M. A. Novak, M. G. Pini, A. Rettori, R. Sessoli and A. Vindigni, *Phys. Rev. Lett.*, 2004, **92**, 207204; L. Bogani, R. Sessoli, M. G. Pini, A. Rettori, M. A. Novak, P. Rosa, M. Massi, M. Fedi, L. Giuntini, A. Caneschi and D. Gatteschi, *Phys. Rev. B: Condens. Matter Mater. Phys.*, 2005, **72**, 064406; N. L. Johnson and S. Kotz, *Distributions in Statistics*, J. Wiley & Sons, New York, USA, 1972.
- 21 M. Bockrath, W. Liang, D. Bozovic, J. H. Hafner, C. M. Lieber, M. Tinkham and H. Park, *Science*, 2001, **291**, 283–285; P. L. McEuen, M. Bockrath, D. H. Cobden, Y. G. Yoon and S. G. Louie, *Phys. Rev. Lett.*, 1999, **83**, 5098–5101.
- 22 G. Dresselhaus, P. Avouris (Ed), *Carbon Nanotubes: Synthesis, Structure, Properties and Application*, Springer-Verlag, Berlin-Heidelberg, 2001; J.-C. Charlier, X. Blase and S. Roche, *Rev. Mod. Phys.*, 2007, **79**, 677–733.
- 23 S. Reich, C. Thomsen, J. Maultzsch, *Carbon Nanotubes: Basic concepts and Physical Properties*, Wiley-VCH, Weinheim, 2004; A. Loiseau, P. Launois, P. Petit, S. Roche, J.-P. Salvetat (ed.), *Understanding Carbon Nanotubes: From Basics to Applications*, Springer-Verlag, Berlin-Heidelberg, 2006.
- 24 C. Gómez-Navarro, P. J. De Pablo, J. Gómez-Herrero, B. Biel, F. J. Garcia-Vidal, A. Rubio and F. Flores, *Nat. Mater.*, 2005, **4**, 534–539; A. V. Krasheninnikov, K. Nordlund and J. Keinonen, *Phys. Rev. B: Condens. Matter Mater. Phys.*, 2002, **65**, 165423.
- 25 H. J. Choi, J. Ihm, S. G. Louie and M. L. Cohen, *Phys. Rev. Lett.*, 2000, **84**, 2917; S. Latil, S. Roche, D. Mayou and J.-C. Charlier, *Phys. Rev. Lett.*, 2004, **92**, 256805; Ch. Adessi, S. Roche and X. Blase, *Phys. Rev. B: Condens. Matter Mater. Phys.*, 2006, **73**, 125414; A. Lopez-Bezanilla, F. Triozon, S. Latil, X. Blase and S. Roche, *Nano Lett.*, 2009, **9**, 940–944.
- 26 H. Park, J. Zhao and J. P. Lu, *Nano Lett.*, 2006, **6**, 916–919.
- 27 K. Bradley, J. Cumings, A. Star, J.-C. P. Gabriel and G. Gruner, *Nano Lett.*, 2003, **3**, 639–641; W. Kim, A. Javey, O. Vermesh, Q. Wang, Y. Li and H. Dai, *Nano Lett.*, 2003, **3**, 193–198.
- 28 L. Bogani, C. Danieli, E. Biavardi, N. Bendiab, A.-L. Barra, E. Dalcanale, W. Wernsdorfer and A. Cornia, *Angew. Chem., Int. Ed.*, 2009, **48**, 746–750; S. Kyatskaya, J. R. Galàn-Mascàros, L. Bogani, F. Hennrich, H. Rösner, W. Wernsdorfer and M. Ruben, *J. Am. Chem. Soc.*, 2009, **131**, 15143–15151.
- 29 F. J. Kahn, P. S. Pershan and J. P. Remeika, *Phys. Rev.*, 1969, **186**, 891–918.
- 30 *Magnetism in Medicine: a Handbook* (Eds: W. Andrä, H. Nowak) WILEY-VCH, Berlin, Germany, 2006; V. Wagner, A. Dullaart, A. K. Bock and A. Zweck, *Nat. Biotechnol.*, 2006, **24**, 1211–1217; D. Pantarotto, J.-P. Briand, M. Prato and A. Bianco, *Chem. Commun.*, 2004, 16–17; N. W. S. Kam, T. C. Jessop, P. Wender and H. Dai, *J. Am. Chem. Soc.*, 2004, **126**, 6850–6851.
- 31 H. Shimada, K. Ono and Y. Otuka, *J. Appl. Phys.*, 2003, **93**, 8259–8264.
- 32 A. K. Geim and K. S. Novoselov, *Nat. Mater.*, 2007, **6**, 183–191.
- 33 L. Bogani, L. Cavigli, K. Bernot, R. Sessoli, M. Gurioli and D. Gatteschi, *J. Mater. Chem.*, 2006, **16**, 2587–2592; E. Cariati, R. Macchi, D. Roberto, R. Ugo, S. Galli, N. Casati, P. Macchi, A. Sironi, L. Bogani, A. Caneschi and D. Gatteschi, *J. Am. Chem. Soc.*, 2007, **129**, 9410–9420; L. Bogani, A. Vindigni, R. Sessoli and D. Gatteschi, *J. Mater. Chem.*, 2008, **18**, 4750–4758; E. Cariati, R. Macchi, E. Tordin, R. Ugo, L. Bogani, A. Caneschi, P. Macchi, N. Casati and A. Sironi, *Inorg. Chim. Acta*, 2008, **361**, 4004–4011; P. L. Gentili, L. Bussotti, R. Righini, A. Beni, L. Bogani and A. Dei, *Chem. Phys.*, 2005, **314**, 9.
- 34 L. Bogani, L. Cavigli, M. Gurioli, R. Novak, M. Mannini, A. Caneschi, F. Pineider, R. Sessoli, M. Clemente-Léon, E. Coronado, A. Cornia and D. Gatteschi, *Adv. Mater.*, 2007, **19**, 3906–3911.